Fuel 354 (2023) 129434

Contents lists available at ScienceDirect

Fuel

journal homepage: www.elsevier.com/locate/fuel

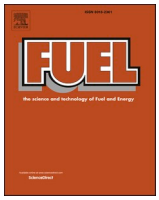

Full Length Article

Numerical investigation on the use of Dimethyl Ether (DME) as an alternative fuel for compression-ignition engines

Andrea Schirru [a,*], Tommaso Lucchini [a], Gianluca D'Errico [a], Marco Mehl [b], Thomas Hilfiker [c], Patrik Soltic [c]

[a] Department of Energy, Politecnico di Milano, Via Lambruschini, 4 20156 Milano, Italy
[b] CRECK Modeling Lab, Department of Chemistry, Materials, and Chemical Engineering, Politecnico di Milano, Italy
[c] Empa, Swiss Federal Laboratories for Materials Science and Technology, Überlandstrasse 129, 8600 Dübendorf, Switzerland

ARTICLE INFO

Keywords:
Dimethyl Ether
Computational Fluid Dynamics
Compression-Ignition Engine
Premixed-Charge Compression-Ignition

ABSTRACT

Dimethyl Ether (DME) is an oxygenated fuel that could favour the transition of the heavy-duty transportation sector to carbon neutrality thanks to its similarities in terms of thermophysical properties with diesel fuel, which will facilitate the retrofitting of existing architectures, and the possibility to achieve good trade-offs between NO_x emissions, soot formation and overall combustion efficiency. The possibility of producing it from a multitude of carbon–neutral sources and the low hydrogen-to-carbon ratio would allow for an overall lower CO2 output, making an attractive option in limiting the global warming impact of the heavy-duty transportation sector. In the present work, a numerical analysis of the combustion process of DME is carried out. First, the numerical setup is validated against experimental data available for a constant volume vessel with an initial density of 14.8 kg/m^3, discussing the capabilities of a chemistry-based combustion model using tabulated kinetics of homogeneous reactors: the Tabulated Well Mixed (TWM) model. Ignition delay times (IDT) are compared for a wide range of temperatures, from 750 K to 1100 K, and oxygen concentrations, from 15% to 21%. The same setup is then applied in the simulation of a heavy-duty internal combustion engine (ICE). A first validation was done to assess the performance of the numerical methodology in a traditional Mixing Controlled Compression Ignition (MCCI) scenario. Then, two other points were simulated: an MCCI condition with 35% of EGR and a Late-Premixed Charge Compression Ignition (L-PCCI) one, with 35% of EGR and an SOI_e of 4 CAD aTDC. Local temperature distributions were compared, analyzing the effect of these technologies in NO_x emission mitigation and their impact on gross indicated efficiency (η_g), showing the advantages that using DME can have on a real-world application.

1. Introduction

With Euro-7/VII regulations expected to become effective from 2027 for heavy-duty vehicles [1], internal combustion engines will be subjected to more stringent limitations regarding exhaust emissions. The smallest particulate matter (PM) to be measured will go from 25 nm to 10 nm while reducing the allowed PM mass by 39% for buses and lorries. NO_x emissions will also be strongly affected, with their maximum concentration limited to just 56% of what was allowed by Euro-6/VI standards while a dedicated limitation will be imposed on nitrous oxide (N_2O) and formaldehyde (CH_2O) for their high greenhouse gas (GhG) potential [2]. Alternative fuels are considered a possible solution for emission mitigation as they can achieve good trade-offs between NOx emissions and PM formation [3,4]. Dimethyl Ether (DME) is an oxygenated fuel producible from a multitude of carbon–neutral sources [5,6]. The complete absence of carbon-to-carbon bonds discourages the formation of particulate matter during combustion and its high oxygen content, 34.8% in mass, prevents the onset of pyrolytic reactions, responsible for soot formation, and favours the complete oxidation of the fuel [7–11]. These characteristics will not only limit the production of soot in diesel-like conditions but would also allow operation with low-temperature combustion modes making it possible to achieve a more favourable trade-off between NO_x emissions and specific fuel consumption [12]. Premixed Charge Compression Ignition (PCCI) is a low-temperature combustion strategy in which a large amount of the injected fuel is already premixed when the ignition event starts. Two main variations of such strategy have been developed: Early-PCCI [13], in

* Corresponding author.
E-mail address: andrea.schirru@polimi.it (A. Schirru).

https://doi.org/10.1016/j.fuel.2023.129434
Received 16 May 2023; Received in revised form 26 July 2023; Accepted 4 August 2023
Available online 7 August 2023

Nomenclature

η_g	Gross Indicated Efficiency
A/F st	Stoichiometric Air-Fuel Ratio
AHRR	Apparent Heat Release Rate
aTDC	After Top Dead Center
BMEP	Brake Mean Effective Pressure
CAD	Crank Angle Degree
CFI	Cool-flame ignition
CI	Compression-Ignition
CN	Cetane Number
DME	Dimethyl Ether
EGR	Exhaust Gas Recirculation
EVO	Exhaust Valve Opening
GhG	Greenhouse Gas
HTI	High-temperature ignition
ICE	Internal Combustion Engine
IDT	Ignition delay times
IVC	Intake Valve Closing
LHV	Lower Heating Value
L-PCCI	Late-Premixed Charge Compression Ignition
MCCI	Mixing Controlled Compression Ignition
NO_x	Nitrogen Oxides
PCCI	Premixed Charge Compression Ignition
PM	Particulate Matter
RANS	Reynolds Averaged Navier-Stokes
SOI_e	Electric Start of Injection
TCR	Critical Temperature
TWM	Tabulated Well Mixed
Z	Mixture Fraction

which the injection event is significantly advanced compared to the top dead center, and Late-PCCI [14], whose injection is delayed after the top dead center. While the latter is known to better mitigate pollutant emissions, it is usually discarded when employing conventional fuels as it drastically increases the risk of wall impingement, which may increase soot and unburnt hydrocarbons. Since DME evaporates faster compared to diesel fuels due to its low boiling point and vapour pressure, it is the perfect candidate for L-PCCI combustion as the likelihood of impinging the combustion chamber's walls is negligible compared to traditional fuels. Moreover, having a lower carbon-to-hydrogen ratio compared to more complex hydrocarbons allows for a smaller amount of CO_2 to be released during combustion [15], reducing the carbon footprint of DME-powered engines.

Table 1 shows that DME has a higher cetane number (CN) compared to diesel fuel and this makes it attractive for compression ignition engines. However, it has a reduced lower heating value and this requires modifications to the entire injection system since a larger amount of fuel should be delivered [16]. Moreover, to compensate for DME's high bulk modulus, a more powerful high-pressure pump is needed to reach the desired injection pressure while additional lubrication must be supplied to compensate for the lower viscosity compared to diesel [17].

There are several examples in the literature illustrating that DME could successfully replace diesel in CI engines. The first experiments were performed on a heavy-duty engine in 1998 [18] where it was possible to achieve smokeless combustion with similar efficiencies to the original diesel engine. Improving existing injection systems or optimizing them for DME use [19–21] could reduce NO_x emissions by up to 40% compared to their diesel counterpart while meantime achieving better fuel consumption. In [22], light and heavy-duty trucks were tested with DME as a fuel for more than 100′000 km, achieving lower exhaust emissions with low compression ratio engines experiencing the biggest gains. The use of DME has been investigated also in alternative combustion modes ranging from Homogeneous Combustion Compression Ignition (HCCI) [23,24], to stoichiometric combustion [25], to dual-fuel configurations in both spark-ignited (SI) [26,27] and compression-ignited (CI) [28] engines.

While experiments are surely crucial to show the real-life potential of a new technology, numerical tools allow to speed up the design process, enable a deeper understanding of the complex fluid dynamics involved in engine combustion and make it possible to perform preliminary investigations to exploit the full potential of DME in terms of combustion chamber design, injection strategy and operating conditions. Although, in the last decade, the available numerical tools have become more and more capable of predicting the real-life behaviour of an internal combustion engine, most combustion models have been developed and validated for engines using conventional fuels that may present evaporative and reacting features that can largely differ from the ones of alternative fuels. This work performs a CFD investigation of DME-fueled engines, focusing attention on both conventional CI and low-temperature combustion. The need to predict properly the ignition delay time and heat release rate during mixing-controlled combustion requires investigating both the effects of the kinetic mechanism and combustion model. Three different kinetic mechanisms were tested [29–31] using the tabulated well-mixed (TWM) combustion model. Constant-volume vessel experiments were used to evaluate the different tested kinetic mechanisms by comparing computed and measured ignition delay data with temperatures ranging from 750 K to 1100 K and oxygen concentrations from 15% to 21% [32]. The validated numerical setup was then applied for combustion simulations in an 11-litres heavy-duty engine. An MC operating condition was validated against experiments before investigating the effect that high EGR rates and Late-Premixed Charge Compression Ignition (L-PCCI) could have on engine efficiency and NO_x production. Finally, the trade-offs of such technology and the potential of using DME to meet the emission standards required for the next generation of engines were discussed.

2. Numerical setup

2.1. Turbulence and spray modeling

CFD simulations were carried out using the open-source code OpenFOAM with Lib-ICE set of dedicated libraries. Turbulence was modelled with a RANS approach with the two-equation model $k-\varepsilon$ [33], with the modified C_1 constant to account for the round jet correction [34]. A Lagrangian approach was used to model the fuel injection where the parcels are distributed inside a solid cone whose angle

Table 1
Thermo-chemical properties of dimethyl ether and diesel where ρ_{liquid} is the liquid density, T_{CR} is the critical temperature, LHV is the lower heating value, ν is the kinematic viscosity and A/F st is the mass-based stoichiometric air–fuel ratio.

	LHV MJ/kg	A/F st -	CN -	ρ_{liquid} kg/m^3	TCR °C	Boiling Point °C	Bulk Modulus Pa	ν mm^2/s
DME	28.8	8.97	55	663	130	−25	6.40E + 08	0.15
diesel	42.8	14.71	45—50	834	450	180–370	1.49E + 09	0.3

was calculated with the correlation suggested in [35]. The breakup of the liquid droplets is simulated using the KH-RT breakup model [36], considering two different breakup regimes: Kelvin-Helmholtz and Rayleigh-Taylor. Given the axial symmetry of the constant volume vessel, a 2-D mesh was used to model the domain. The resulting mesh consists of 20 K cells with a minimum cell size along the injector axis of 0.2 mm. The mesh was refined along the injection direction, with cells that become gradually bigger, farther from the injection axis. This is done to contain the overall computational cost of the simulation while still having a detailed enough description of the fluid region where the injection event takes place.

2.2. Combustion modeling

To model the combustion process, the Tabulated Well Mixed (TWM) model was selected. As the name suggests, this tabulated approach is based on the assumption that every cell in the CFD domain can be considered a perfectly homogeneous reactor. This model solves the chemistry problem separately from the fluid-dynamic one and accesses information on the combustion advancement from a lookup table where the reaction rates and the species evolution during the process are stored. The lookup table is generated by storing the solution of homogeneous reactor simulations for several operating conditions, covering all possible thermodynamic conditions found locally inside the engine's combustion chamber.

The process starts by specifying the reactors' initial conditions based on pressure, initial temperature, equivalence ratio and EGR (Fig. 1). Once all the reactors are initialized, auto-ignition simulations are performed, using the specified kinetic scheme to calculate the chemical species' reaction rates:

$$\frac{dY_i}{dt} = \dot{\omega}_i(T, p, Y_1, \cdots, Y_n) \tag{1}$$

where Y_i is the i-th species' mass fraction, and $\dot{\omega}_i$ is the i-th species' reaction rate.

Data inside the table are stored as a function of a combustion progress variable defined as the total amount of heat released during combustion [37]:

$$C = \sum_{i=1}^{N_s} h_{298,i} Y_i(t) - \sum_{i=1}^{N_s} h_{298,i} Y_i(0) \tag{2}$$

where $h_{298,\,i}$ is the enthalpy of formation of the i-th species and N_s is the total number of species defined in the kinetic mechanism. A normalized version of the progress variable (c) can be calculated by estimating the progress variable in equilibrium conditions (C_{max}) and its initial value (C_{min}):

$$c = \frac{C - C_{min}}{C_{max} - C_{min}} \tag{3}$$

and its reaction rate can be calculated as:

$$\dot{c} = \frac{c_{i+1} - c_i}{t_{i+1} - t_i} \tag{4}$$

The CFD solver accesses the table during runtime to extract the source term of the progress variable's transport equation reported below:

$$\frac{\partial \overline{\rho \tilde{C}}}{\partial t} + \nabla\left(\overline{\rho \tilde{U} \tilde{C}}\right) - \nabla\left(\frac{\tilde{\mu}_t}{Sc_t} \nabla \tilde{C}\right) = \rho \dot{C} \tag{5}$$

Giving every cell in the domain the possibility to evolve independently, it is very sensitive to the local flow conditions, favouring the prediction of a gradual ignition of the air–fuel mixture and giving it the ability to predict several flame behaviours such as stabilization and recess.

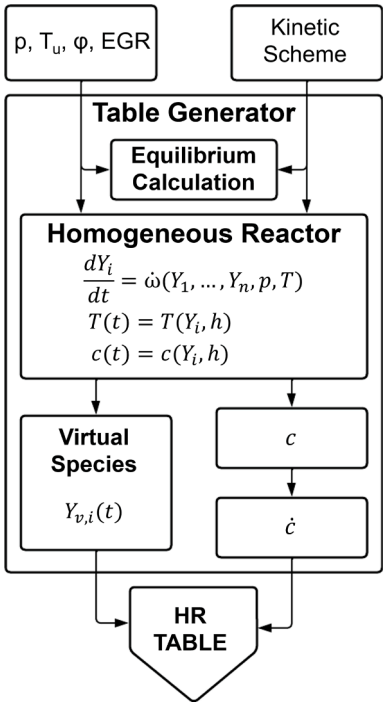

Fig. 1. Schematic representation of the generation procedure of the look-up table.

3. Validation of the numerical method

3.1. Kinetic mechanisms

Since the selected combustion model will be largely affected by the kinetic scheme selected to model DME's oxidation process, a brief analysis of some of the available mechanisms in the literature was carried out comparing IDT predicted in a wide range of ambient conditions. Experimental data from Burke et al. [38] were selected for their high-pressure characteristics and the presence of both stoichiometric and rich conditions. The complete set of conditions can be found in Table 2. Auto-ignition simulations were carried out in non-isothermal constant volume homogeneous reactors using the OpenSMOKE++ framework [29], where the IDT was then estimated as the moment at which the maximum pressure increase is registered inside the domain, coherently with what was done for experiments. Three different mechanisms were considered for the comparison: Livermore's (LLNL) [30], the ARAMCO 1.3 C4 [31] and CRECK's [39,40] (Table 3).

Results from the comparison can be seen in Figs. 2 and 3. Starting with the cases at 11.5 atm (Fig. 2), all mechanisms seem to perform similarly for temperatures above 1000 K while some differences can be observed at lower temperatures, where the LLNL better interpolates the experimental data and CRECK and ARAMCO are respectively underestimating and overestimating the IDT.

The LLNL mechanism presents a slightly irregular behaviour in the negative temperature coefficient region, where the simulated line shows a different trend compared to the other two models, with an almost linear increase in IDT with decreasing temperatures. Similar differences between the mechanisms can be observed at higher pressures, where ARAMCO and CRECK behave more similarly, while LLNL's agreement with experiments worsens compared to the lower pressures, in particular

Table 2
Operating conditions simulated for the kinetic mechanism's comparison.

Pressure	Temperature	Equivalence Ratio
[atm]	[K]	[-]
11.0 – 25	680 – 1350	1.0 – 2.0

Table 3
Kinetic mechanisms used for IDT comparison. For each mechanism the year of publication, the number of species and reactions are reported.

	Publication Year	N. species	N. reactions
LLNL	2004	84	355
ARAMCO	2014	116	713
CRECK	2022	177	2858

at lower temperatures. In Figs. 4 and 5, reactivity maps of the three mechanisms are presented. Along the x-axis, the Mixture Fraction (Z), defined as the mass fraction of fuel, is reported, covering ranges from lean to rich conditions, where the stoichiometric value can be found in the neighbourhood of 0.1 for DME. On the y-axis, the normalized progress variable gives information on the completion status of the conversion process while its reaction rate is used to color the map to visualize the different reactivity of the mixtures.

For all three mechanisms, two distinct regions can be identified:

7. Cool-flame ignition (CFI): it can be identified as the isolated reactivity zone in the lower part of the graph ($c < 0.4$).

8. High-temperature ignition (HTI): identified as the bigger reactivity "island", where the higher reaction rates are found (c greater than 0.4).

A single pressure of 20 bar and two different temperatures (750 K and 1100 K) were selected, to study the behaviour of the mechanism at both low and high temperatures. Starting with the low-temperature condition (Fig. 4), the CFI region looks very prominent for all the mechanisms, extending from the lean to the rich region.

This phenomenon is attributed to the hydroperoxy alkyl radicals branching, which is known to be the leading phenomenon in the auto-ignition process of oxygenated organic compounds [41]. This is a dominant behaviour at lower temperatures where reactions with high activation energy struggle to start. At high temperatures, as can be seen from Fig. 5, the CFI region can be found only in extremely rich regions where branching phenomena stay relevant for the ignition process. As for the differences between mechanisms, we can see that the lower temperature regime is the one in which they present the larger differences. CRECK shows a significantly higher reactivity in the CFI region compared to the other two, which increases the conversion speed, resulting in shorter ignition delay times. This seems to be true for the whole range of tested equivalence ratios where ARAMCO and LLNL have similar characteristics, with the first one showing slightly higher reaction rates. Such observations are confirmed from Fig. 3a and b where LLNL has a longer IDT compared to ARAMCO in the low-temperature region. In the high- temperature condition, differences in reactivity are smaller for the three mechanisms which show similar reaction rates in the lean-to-stoichiometric region ($Z < 0.1$). In richer regions, CRECK seems once again to be the most reactive, followed by ARAMCO and LLNL.

ARAMCO and c) LLNL.

3.2. Constant-Volume vessel simulations

A further comparison of the three mechanisms was carried out in a

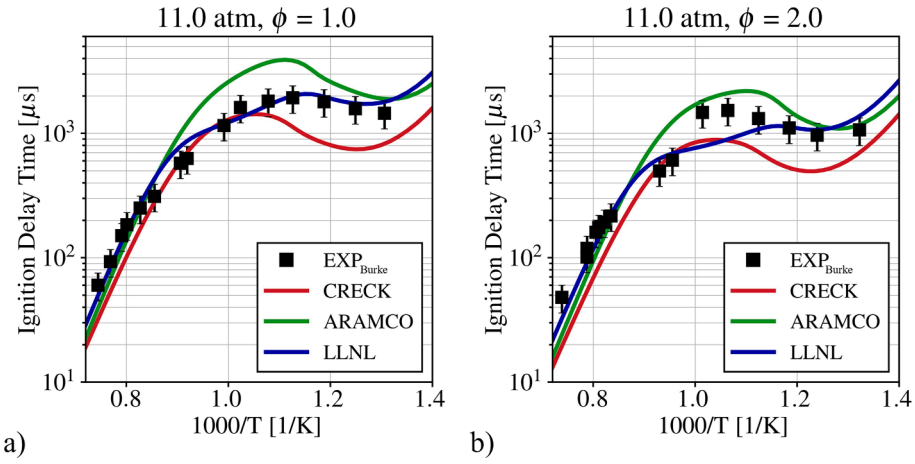

Fig. 2. Ignition delay time comparison between experiments [32] and simulations at 11.0 atm.

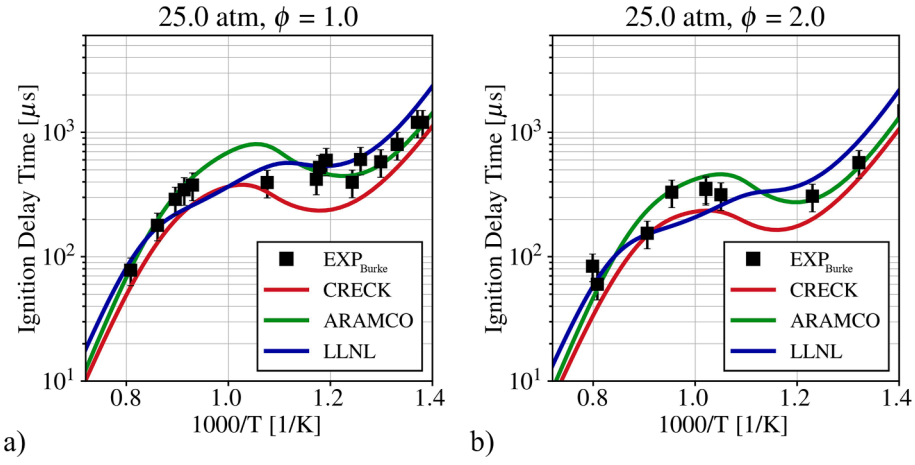

Fig. 3. Ignition delay time comparison between experiments [32] and simulations at 25.0 atm.

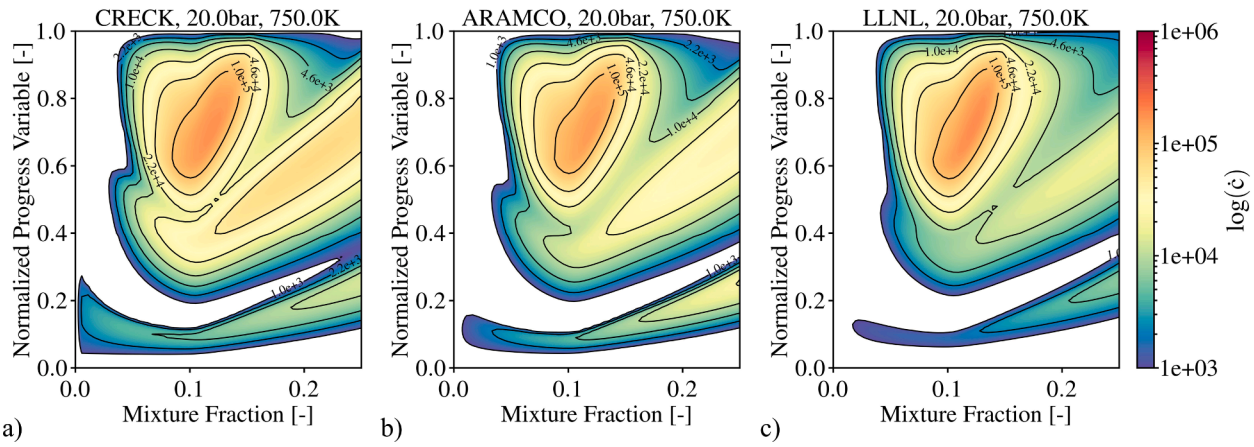

Fig. 4. Reactivity maps (expressed in terms of progress variable reaction rate) for an operating condition at 20 bar and 750 K for a) CRECK, b) ARAMCO and c) LLNL.

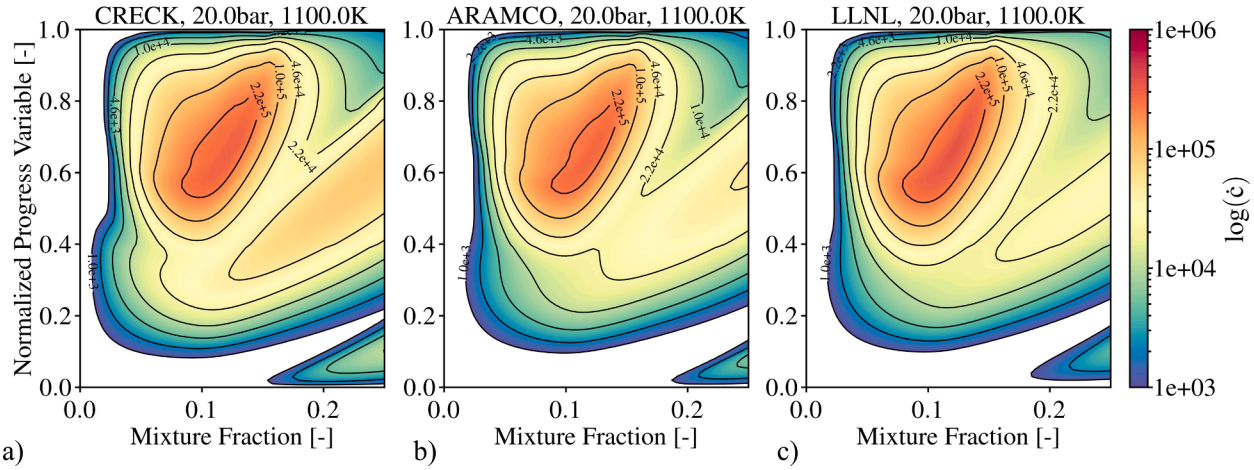

Fig. 5. Reactivity maps (expressed in terms of progress variable reaction rate) for an operating condition at 20 bar and 1100 K for a) CRECK, b) ARAMCO and c) LLNL.

2D constant-volume vessel, using the TWM combustion model. To consistently compare the simulated results with the available experimental data [32] (Table 4), the IDT was defined as the difference between the ignition time and the start of injection (SOI):

$$IDT = t_{ignition} - t_{SOI} \tag{6}$$

where $t_{ignition}$ was defined as the moment at which the maximum increase in temperature is registered (Eq. (7):

$$t_{ignition} = t\left(max\left(\frac{dT}{dt}\right)\right) \tag{7}$$

with t being the time and T the temperature.

Table 4
Simulated operating conditions. The "Exp. Data" column checks the availability of the experimental IDT.

Density [kg/m^3]	T [K]	O_2 [%vol]	Exp. Data
		15	
	750	18	X
		21	
		15	X
14.8	900	18	X
		21	X
		15	
	1100	18	X
		21	

A first comparison is proposed in Fig. 6a where the sensitivity of the numerical setup to a variation of the initial temperature was tested while keeping the initial oxygen concentration at 18%. While all kinetic schemes were capable of correctly predicting the increase in IDT due to a decrease in temperature, an underprediction of the experimental value is observed for most of the simulated points. The mechanisms perform coherently with what was observed in the comparison proposed in the previous paragraphs, with CRECK having the highest reactivity between the three and LLNL igniting the latest. Moreover, ARAMCO and CRECK show a similar sensitivity to the change in ambient conditions while LLNL suffers from a large overestimation of the IDT in the low-temperature condition.

Another series of data was selected to show the sensitivity of the proposed kinetic schemes to the variation of oxygen concentration inside the vessel. This is important to assess the mechanisms' raw performances and gives us a chance to evaluate the numerical setup in a critical scenario. Due to the longer chemical ignition delay caused by a lower oxygen concentration inside the vessel, the ability of the spray model to correctly predict the entrainment of air before the onset of combustion will be emphasized. A comparison between simulation and experiments is shown in Fig. 6b where all the schemes predict an increase of IDT which is almost linear when decreasing the oxygen concentration, consistent with the measured data. Despite the underestimation of the ignition delay times resulting from the use of the TWM model in combination with CRECK and. ARAMCO, it was always possible to correctly predict the dependency of IDT varying ambient

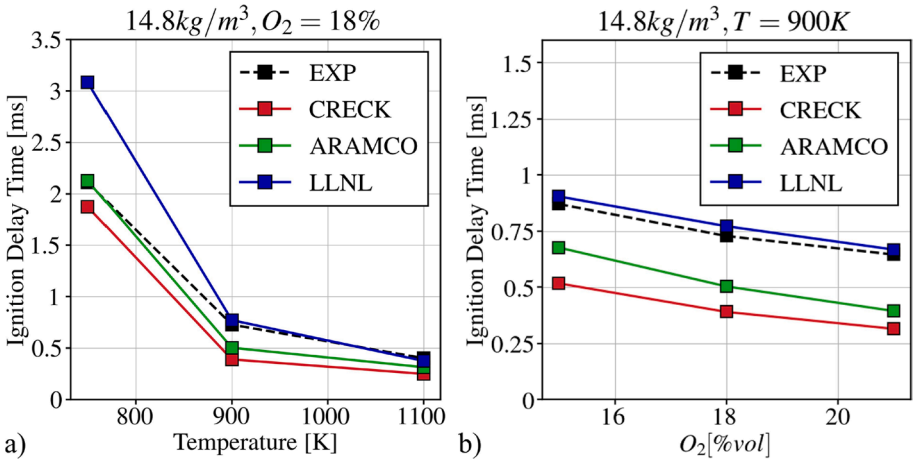

Fig. 6. Comparison of experimental and simulated results in terms of IDT. In a) the oxygen concentration is fixed at 18% and the sensitivity to the ambient temperature is studied. In b) the ambient temperature is fixed at 900 K observing the sensitivity to different oxygen concentrations.

temperature and oxygen concentration.

From the results in Fig. 6, we conclude that all three setups are sensitive to temperature and oxygen concentration variation with the newer schemes (ARAMCO and CRECK) performing similarly to each other and LLNL reporting overall a better agreement with this set of experiments except for low temperature conditions. Before proceeding with the engine simulations, a preliminary test was carried out imposing the ambient conditions that will be found inside the engine in the three operating conditions selected for the investigation (Table 5).

As expected, a similar trend as the previously presented results is shown in Fig. 7 where we can see a negligible difference in the predicted IDT for ARAMCO and CRECK while LLNL shows once more a lower reactivity. Being CRECK and ARAMCO more recently developed compared to LLNL, the validation database on the base of which they were developed is larger and more extended in terms of operating conditions compared to LLNL. For this reason, for conditions outside the validated range, LLNL prediction of the experimental behaviour is not satisfactory as was proven by looking at the low-temperature conditions in Figs. 3 and 6. Since a key point of the following section will be the prediction of NO_x emissions in engine simulation, the selection of the preferred mechanism took into consideration the possibility of the analyzed schemes to model the NO_x formation process. While a set of equations to model the formation of such pollutant could be added to any given mechanism, this methodology was already tested by the authors in previous works achieving a rather unsatisfactory accuracy when compared with the experimental values in the estimation of the amount of NO_x produced by the engine [16]. More recently, using CRECK in similar operating conditions an improved agreement was achieved in this regard[42]. Moreover, since a tabulated approach is selected to model combustion, the computational cost of the simulation is not affected by the number of species and reactions that compose the kinetic scheme hence the use of a reduced mechanism does not provide considerable advantages in terms of computation time. For these reasons, CRECK will be employed in the following section to model the combustion of a heavy-duty compression ignition engine powered by DME.

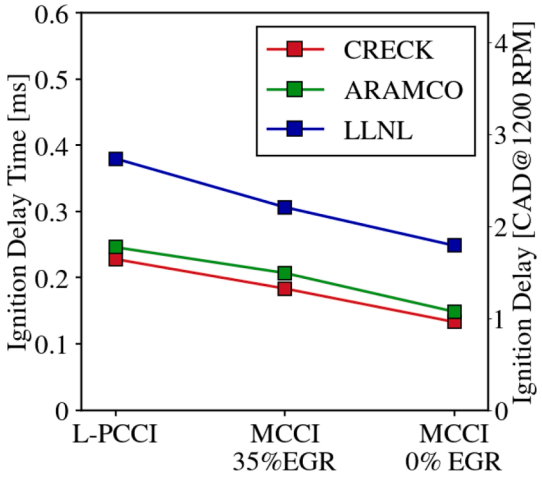

Fig. 7. Ignition delay times comparison between three different mechanisms in ambient conditions similar to the one found at the start of injection of the engine points considered for the investigation.

3.3. Engine simulations

A numerical analysis was carried out on a heavy-duty engine operating with DME, whose main geometrical characteristics are reported in Table 6. The experimental database was extracted at EMPA's laboratories where a test bench using a Horiba Dynas3 HD 600 dynamometer was used while a Horiba Mexa 7500 DEGR was capturing the exhaust

Table 5
Operating conditions considered for engine simulations and respective NO_x emission values.

Name	SOI_e [CAD aTDC]	Exp. NO_x [ppm]	Sim NO_x [ppm]	Fuel Mass [mg/cycle]	GIE [%]
MCCI 0% EGR	−6.8	522.9	440.5	101.84	45.42
MCCI 35% EGR	−6.8	83	52.4	105.12	42.41
L-PCCI 35% EGR	4	37	29.0	117.04	36.00

Table 6
Main geometrical characteristics of the engine.

Displacement Volume	11000 cm^3
Stroke	144 mm
Bore	128 mm
Connecting Rod Length	228 mm
Compression Ratio	20.5:1
Number of Valves (per Cylinder)	4
Piston Bowl Shapes	Re-entrant, H type
Exhaust Valve Opening (EVO)	123 CAD aTDC
Intake Valve Closing (IVC)	143 CAD bTDC

emissions. To reduce the computational cost of the simulation, only the closed-valve part of the engine cycle was considered. Initial and boundary conditions were taken from a previously validated 1D model of the engine [16] and, taking advantage of the combustion chamber's symmetry, 1/8 of the fluid-dynamic domain was simulated. The resulting sector mesh (Fig. 8), was generated with the same approach described in [43]. The mesh generator takes as an input the digitized profile of the combustion chamber in the form of a VTK or CSV file. From the 2D mesh, represented in Fig. 8b, the 3D mesh is generated, specifying the sector angle and the number of cells in the tangential direction. With this approach, a fully hexahedral spray-oriented mesh can be generated resulting in a high-quality representation of the interaction between the fuel jet and the flow field in the combustion chamber.

For the simulations proposed in the present work, the mesh is composed of 100 K elements at TDC which was the minimum number of elements to achieve mesh independence of the results. An instrumented injector was used to measure the needle lift profile and the injection pressure (which was fixed at 570 bar), allowing to record the experimental mass flow rate and estimate the hydraulic delay. The TWM model was used, for which a homogeneous reactor table was generated with 7 pressures, 16 temperatures and 45 equivalence ratios, resulting in 5040 auto-ignition simulations. The complete set of tabulated conditions is reported in Table 7.

A first simulation was done to assess the behaviour of the numerical setup and compare it with the available experimental data. The engine was operated in Mixing Controlled Compression Ignition (MCCI) conditions with a SOI_e = -6.8 CAD before-Top Dead Center (bTDC), and 0% of external EGR. From a first comparison, shown in Fig. 9, the TWM model shows a good prediction of the ignition delay as well as of the mixing-controlled phase of the combustion process compared to experiments. The reported pressure curve is derived from the averaging of 200 consecutive cycles. While powering internal combustion engines with oxygenated fuels can sometimes increase the cycle-to-cycle variability, as reported in [44], it was not the case for the considered operating conditions. As for the estimation of the release of heat during the combustion process, a coherent methodology was applied to experiments and simulations, utilizing the same heat capacity ratio for both.

A small over-prediction of the peak cylinder pressure is observed compared to experiments which are thought to be due to a contained overestimation of the in-cylinder pressure at SOI, probably caused by small uncertainties in the ambient conditions at IVC and by the imposed wall temperatures derived from the 1D model. However, given the entity of such difference compared to the absolute value of the peak pressure, the agreement can be considered satisfactory for the selected operating condition. A more detailed validation of the used numerical setup can be found in [16] where the authors carried out an extended numerical campaign over a vast range of operating conditions with different loads, SOI_e and injection pressure. To study the effect of high EGR levels and L-PCCI two additional points were numerically investigated. The L-PCCI condition selected for comparison was taken from the experimental database as the one with the larger reduction of NO_x emissions which is still capable of stability operate. All the points have the same load, with a Brake Mean Effective Pressure (BMEP) of 6.8 bar and an engine speed of 1200 rpm. All the studied conditions have been summarized in Table 5, reporting Electrical Start of Injection (SOI_e) efficiency and NO_x emissions. In Fig. 9, a comparison between two operating conditions having the same SOI_e and different EGR rates is reported. The first one is the base case (MCCI 0% EGR) just described, whose agreement concerning experiments is shown, while the second one is characterized by a global EGR ratio of 35%. The first noticeable difference is that the two considered conditions have different in-cylinder pressures at SOI_e and in particular, the case with a higher EGR rate has a higher pressure compared to the base case. Such behaviour could seem counter-intuitive since the polytropic index of pure air is surely larger than the one containing a certain percentage of exhaust gases, which should result in a higher pressure at the end of the compression stroke for the base case. Although this is theoretically correct, it is based on the assumption that both points have the same pressure at Intake Valve Closing (IVC) which is not the case for these two points. To maintain a similar amount of oxidizer between the two cases, a larger intake pressure should be

Table 7
Operating conditions used to generate the homogeneous reactor table.

	Range	Number of Values
Pressure	10 – 200 bar	7
Temperature	400 – 1250 K	16
Fuel Mass Fraction	0 – 1	45

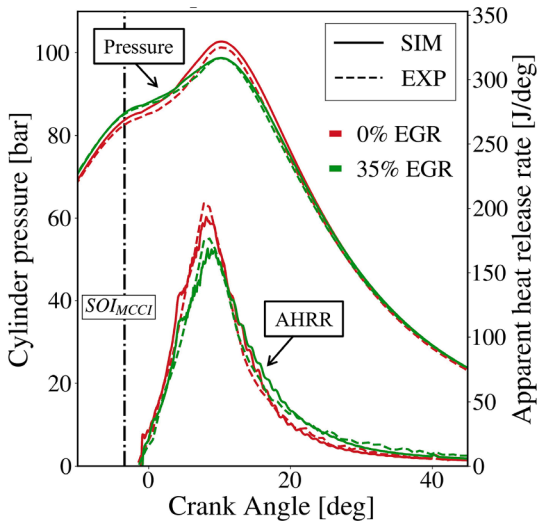

Fig. 9. Engine simulation validation of two operating conditions with 6.8 bar of BMEP at 1200 rpm. The red one is with 0% EGR while the green one has 35%. Both conditions have the same electric SOI equal to −6.8 CAD aTDC.

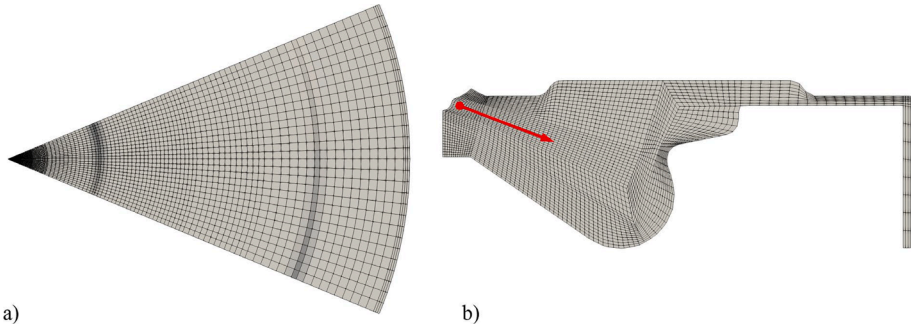

Fig. 8. a) Top view and b) lateral section view of the sector mesh used for engine simulations.

imposed on the case with EGR, to account for the presence of the exhaust gases, which will not take part in the combustion process. A slightly longer ignition delay is experienced for the case with EGR as well as an overall slower combustion process for the base case, which causes a larger part of the heat to be released during the expansion stroke. While a larger difference in terms of IDT could be expected between the 0% and 35% EGR cases due to the different dilution levels, the in-cylinder conditions at the start of injection for the two cases are not identical. The simulated average and maximum temperatures recorded during combustion are reported in Fig. 10. The 35% EGR case reports higher temperatures at the SOI which, together with the higher pressure, lowers the effective IDT not only accelerating the evaporation of the fuel but also decreasing the expected chemical ignition delay time. Focusing on the local effect of using a high EGR rate, it can be observed from Fig. 11a how the local temperature distribution affects the NOx formation. The timestep at 2.5 CAD aTDC was selected since it presents a fully developed spray jet which has not yet interacted with the piston walls. The image was divided into two with the top part representing the base case and the bottom part having 35% of EGR. Finally, an *iso*-surface was reported in white, containing the region having a NOx concentration higher than 2 ppm. From the contour plot, it can be seen how the lower local temperatures of the case with EGR drastically lower the NOx production during combustion. From Fig. 11b, the effect just described can be qualitatively appreciated. For both cases, a similar trend is observed, with the peak production of NO_x being around the stoichiometric mixture fraction value Z_{st} (identified by the dash-dotted lines), where maximum temperatures are expected during combustion. Although both cases used pure DME as a fuel, the Z_{st} value differs due to the composition of the mixture inside the combustion chamber, causing the case with EGR to have a maximum NO_x production for a lower Z value compared to the base case.

A third case, operating in an L-PCCI configuration, was then investigated. With an SOI_e of 4 CAD aTDC, the whole combustion process takes place during the expansion stroke (Fig. 12). As waspreviously discussed for the MCCI case with 35% of EGR, the higher in-cylinder pressure at the end of the compression stroke compared to the base case is due to a higher intake pressure used to achieve similar oxidizer mass between the two cases. A visible difference in the IDT is observed between the base MCCI case and the L-PCCI one. Such a result confirms what was previously found in Fig. 7 where the effect of high EGR rates and lower temperatures were investigated inside the simplified environment of the constant-volume vessel. Moreover, the evaporation process is slowed down due to both the lower temperature of the environment, which causes a delay in the change of phase of the injected fuel, as well as the lower in-cylinder pressures, which reduces the evaporation rate of the fuel droplets due to a reduction in the aerodynamic forces exchanged between the fuel spray and the high-pressure environment found inside the cylinder. In terms of agreement with experiments for the L-PCCI case, the TWM predicts a slightly anticipated onset of combustion which causes a mismatch compared to the experimental curve.

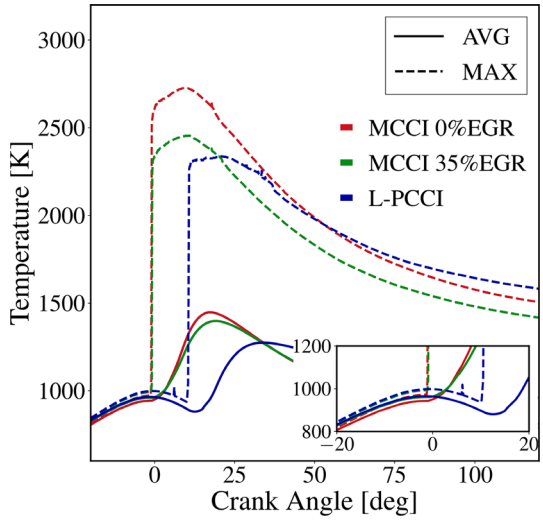

Fig. 10. Simulated in-cylinder average (continuous line) and maximum (dashed line) temperature.

This could be the result of the excessive reactivity showed by CRECK in previous instances (in particular at lower pressures like in this case) as well as limitations of the TWM model in precisely predicting the onset of combustion in complex fluid-dynamic conditions as the one that can be found when the combustion process is developing entirely during the expansion stroke. In terms of NO_x emissions, delaying the SOI_e after the TDC allows for a further reduction of the local temperatures compared to the sole use of EGR as reported in Table 5. However, the combined use of high EGR rates and extreme injection delays causes the phasing of the combustion process to be shifted towards the expansion stroke, resulting in a gross indicated efficiency (η_g) just lower than 40%. From Fig. 13, a visual representation of the trade-off between NO_x and fuel consumption/efficiency is proposed. Two threshold values are proposed: the Euro 6/VI limit, considered as the regulation limit imposed by the European Commission for heavy-duty vehicles, and the Euro 7/VII one, which is a projection of the possible new regulation, which could enforce a 56% reduction of the NO_x emission compared to Euro 6/VI. Since the regulations refer to exhaust emissions measured at the tailpipe, a 90% efficiency of the exhaust after-treatment system was assumed to estimate the regulatory limit at EVO. The NO_x emissions from CFD simulations are first compared with the available experimental measurements. From a numerical point of view, the approach used to model NO_x emissions consists in tabulating the evolution of NO, NO_2 and N_2O based on a dedicated progress variable defined as:

$$C_{NO_x}(t) = \frac{Y_{NO_x}(t)}{Y_{NO_{x,eq}}} \tag{8}$$

where Y_{NOx} and $Y_{NOx,\,eg}$ are respectively the mass fraction of NO_x at a certain timestep and equilibrium. This is done to avoid using the same progress variable used to model the ignition process since the characteristic times for the formation of NO_x emissions are much longer compared with the IDT. Consistently with what is observed from Fig. 13, such methodology tends to underestimate the NOx formation compared to experiments, due to the extreme simplifications introduced by the WM assumption. This behaviour is consistent with what was observed in several other works regarding both traditional and alternative fuels with the same tabulated approach [16,45,46]. In this specific case, the operating condition with the larger underestimation of the CFD predicted data compared with experiments is around 18%. If on one side this is surely not a negligible difference, the sensitivity of the numerical setup to varying ambient conditions was observed to be consistent with experiments, allowing us for a comparison between the different technologies presented in this work.

Evaluating the trade-off between NO_x emissions and efficiency, it seems clear that using high EGR levels could potentially allow for a drastic reduction in emissions with a loss of gross indicated efficiency of 3%, which is 6.6% lower if compared with the baseline case. L-PCCI combustion, combining the effects of high EGR rates and late injections to limit the local temperatures during the combustion process, can almost halve the NO_x emissions achieved by the MCCI 35% EGR case with a further loss in gross indicated efficiency of 6%, 20% lower than the baseline case. While such low-temperature combustion technology could still be effective to achieve a further reduction in overall NO_x emissions, the efficiency loss is too high to justify it. Lower delays of SOI_e should be tested to find the optimal combination between NO_x mitigation and efficiency. Moreover, the dilution levels should undergo a deeper analysis to optimize such a strategy. While an energy analysis

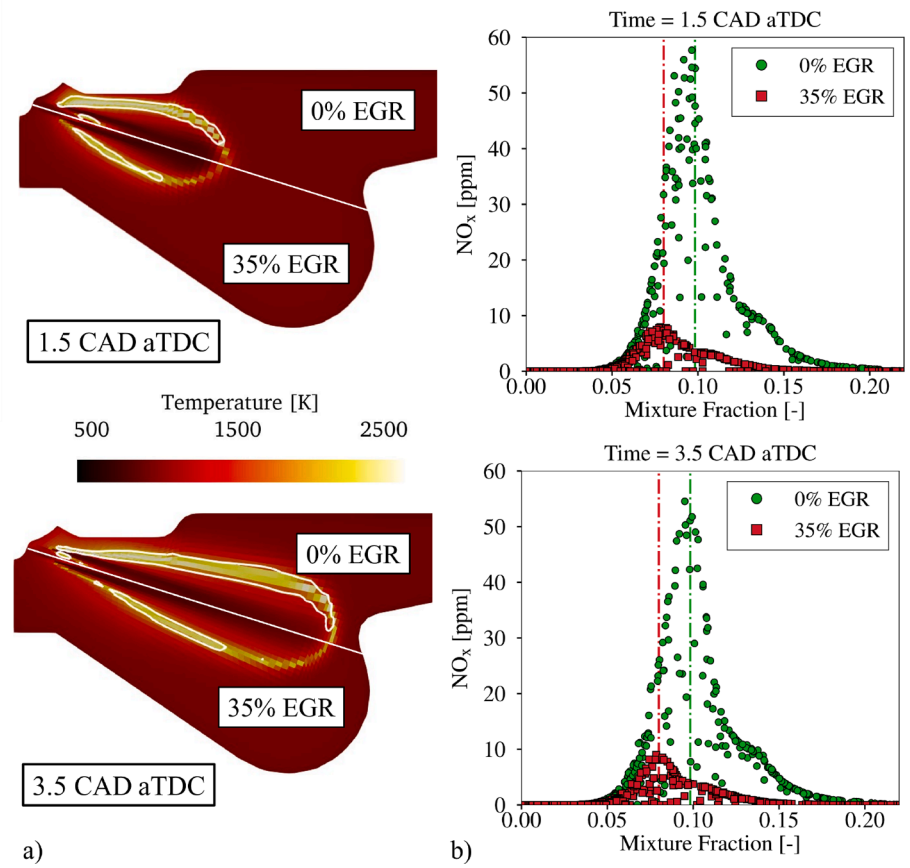

Fig. 11. a) local temperature field for two operating conditions with (bottom) and without (top) egr where the white*iso*-surface represents the region with a NO_x concentration higher than 2 ppm. In b) a scatter plot of the NO_x concentration against the mixture fraction Z is proposed, where the colour-matched dash-dotted lines represent the stoichiometric mixture fraction values for the two cases.

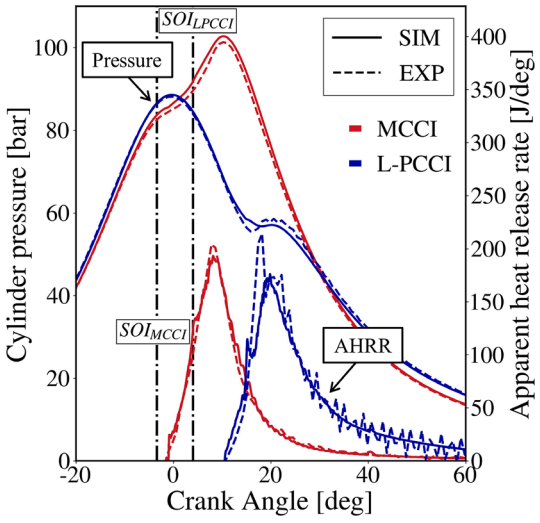

Fig. 12. Comparison of experimental and simulated data in terms of pressure and AHRR for an MCCI and an L-PCCI condition.

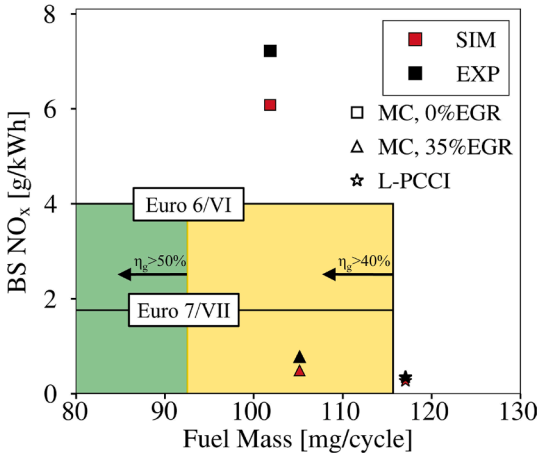

Fig. 13. Trade-off NO_x-Fuel Mass injected per cycle for the operating conditions reported in the paper. The green and the yellow region are regions that comply with the Euro 6/VI regulation and with η_g higher than 50% and 40% respectively.

was carried out in the present work, a clearer understanding of the phenomenon could be provided by analyzing the exergy balance as proposed in [47], allowing the achievement of an optimal trade-off between performance and pollutant emissions limitation.

4. Conclusions and outlook

DME is an alternative fuel which could be a promising replacement for conventional diesel fuel due to its potential in the combined reduction of NO_x and particulate matter, favoured by its high oxygen concentration and evaporative capabilities. In the present work:

- A first investigation on the predictive performances of three kinetic schemes was carried out simulating first a 0D auto-ignition problem in high-pressure conditions before moving to reacting spray simulations where the combined effect of spray and combustion modeling was analyzed.
- A heavy-duty engine operating with DME was then considered to evaluate the use of DME in a compression ignition engine.
- A first validation was carried out on a conventional MCCI condition with no EGR using a tabulated approach based on the well-mixed assumption to model combustion. The numerical setup showed satisfactory results, capturing the main features of the pressure and AHRR curve and correctly predicting their peak values from a quantitative point of view.
- Two other conditions were then simulated to assess the effect of high EGR rates and L-PCCI on the combustion process and the production of NO_x emissions. Both strategies allowed to contain the local temperatures during the combustion process allowing to successfully mitigate the NO_x production. L-PCCI was the most successful in doing so, predicting just 29.0 ppm but it was strongly affected in terms of efficiency due to the extreme delay in SOI_e. The sole use of high EGR rates showed a reduction of NO_x of almost 10 times compared to the base case while keeping similar efficiencies, showing promising results which could facilitate to comply with Euro 7/VII regulations.
- Further optimizations should be carried out to better exploit the fuel characteristics in the mitigation of pollutant emissions while keeping high enough efficiencies to be competitive with more traditional fueling solutions.

CRediT authorship contribution statement

Andrea Schirru: . **Tommaso Lucchini:** Writing – review & editing, Supervision, Methodology. **Gianluca D'Errico:** Writing – review & editing, Supervision. **Marco Mehl:** Supervision, Software, Investigation. **Thomas Hilfiker:** Data curation. **Patrik Soltic:** .

Disclosure statement

Part of the research has received funding from "Ecosystem for Sustainable Transition in Emilia-Romagna", a project funded by European Union under the National Recovery and Resilience Plan (NRRP), Mission 04 Component 2 Investment 1.5—NextGenerationEU, Call for tender n. 3277 dated 30/12/2021, Award Number: 0001052 dated 23/06/2022.

Declaration of Competing Interest

The authors declare that they have no known competing financial interests or personal relationships that could have appeared to influence the work reported in this paper.

Data availability

The authors do not have permission to share data.

References

[1] "Regulation of the european parliament and of the council on type-approval of motor vehicles and engines and of systems, components and separate technical units intended for such vehicles, with respect to their emissions and battery durability (Euro 7) and repealing Regulations (EC) No 715/2007 and (EC) No 595/2009," *European Commission - European Commission*. https://ec.europa.eu/commission/presscorner/detail/en/ip_22_6495 (accessed Nov. 22, 2022).
[2] O. US EPA, "Overview of Greenhouse Gases," Dec. 23, 2015. https://www.epa.gov/ghgemissions/overview-greenhouse-gases (accessed Jul. 21, 2023).
[3] Zhu H, Bohac SV, Nakashima K, Hagen LM, Huang Z, Assanis DN. Effect of fuel oxygen on the trade-offs between soot, NOx and combustion efficiency in premixed low-temperature diesel engine combustion. Fuel Oct. 2013;112:459–65. https://doi.org/10.1016/j.fuel.2013.05.023.
[4] Härtl M, Seidenspinner P, Wachtmeister G, Jacob E. Synthetic Diesel Fuel OME1 A Pathway Out of the Soot-NOx Trade-Off. MTZ Worldw Jul. 2014;75(7):48–53. https://doi.org/10.1007/s38313-014-0173-1.
[5] Lee U, Han J, Wang M, Ward J, Hicks E, Goodwin D, et al. Well-to-Wheels Emissions of Greenhouse Gases and Air Pollutants of Dimethyl Ether from Natural Gas and Renewable Feedstocks in Comparison with Petroleum Gasoline and Diesel in the United States and Europe. SAE Int J Fuels Lubr 2016;9(3):546–57.
[6] Styring P, Dowson GRM, Tozer IO. Synthetic Fuels Based on Dimethyl Ether as a Future Non-Fossil Fuel for Road Transport From Sustainable Feedstocks. Accessed: Nov. 24, 2022. [Online]. Available: Front Energy Res 2021;9. https://www.frontiersin.org/articles/10.3389/fenrg.2021.663331.
[7] Ying W, Longbao Z, Hewu W. Diesel emission improvements by the use of oxygenated DME/diesel blend fuels. Atmos Environ Apr. 2006;40(13):2313–20. https://doi.org/10.1016/j.atmosenv.2005.12.016.
[8] Graboski MS, McCormick RL. Combustion of fat and vegetable oil derived fuels in diesel engines. Prog Energy Combust Sci Jan. 1998;24(2):125–64. https://doi.org/10.1016/S0360-1285(97)00034-8.
[9] Choi CY, Reitz RD. An experimental study on the effects of oxygenated fuel blends and multiple injection strategies on DI diesel engine emissions. Fuel Sep. 1999;78(11):1303–17. https://doi.org/10.1016/S0016-2361(99)00058-7.
[10] Neeft JPA, Makkee M, Moulijn JA. Diesel particulate emission control. Fuel Process Technol 1996;1(47):1–69.
[11] Rakopoulos DC, Rakopoulos CD, Giakoumis EG, Papagiannakis RG. Evaluating Oxygenated Fuel's Influence on Combustion and Emissions in Diesel Engines Using a Two-Zone Combustion Model. J Energy Eng Aug. 2018;144(4):04018046. https://doi.org/10.1061/(ASCE)EY.1943-7897.0000556.
[12] Han J, Wang S, Maria Vittori R, Somers LMT. Experimental study of the combustion and emission characteristics of oxygenated fuels on a heavy-duty diesel engine. Fuel May 2020;268:117219. https://doi.org/10.1016/j.fuel.2020.117219.
[13] T. Kanda, T. Hakozaki, T. Uchimoto, J. Hatano, N. Kitayama, and H. Sono, "PCCI Operation with Early Injection of Conventional Diesel Fuel," presented at the SAE 2005 World Congress & Exhibition, Apr. 2005, pp. 2005-01–0378. doi: 10.4271/2005-01-0378.
[14] T. Kanda, T. Hakozaki, T. Uchimoto, J. Hatano, N. Kitayama, and H. Sono, "PCCI Operation with Fuel Injection Timing Set Close to TDC," presented at the SAE 2006 World Congress & Exhibition, Apr. 2006, pp. 2006-01–0920. doi: 10.4271/2006-01-0920.
[15] "Carbon Dioxide Emission - an overview | ScienceDirect Topics." https://www.sciencedirect.com/topics/chemistry/carbon-dioxide-emission (accessed Jul. 21, 2023).
[16] A. Schirru *et al.*, "Combustion Modeling in a Heavy-Duty Engine Operating with DME Using Detailed Kinetics and Turbulence Chemistry Interaction," presented at the WCX SAE World Congress Experience, Mar. 2022, pp. 2022-01–0393. doi: 10.4271/2022-01-0393.
[17] A. K. Voice, T. Tzanetakis, and M. Traver, "Lubricity of Light-End Fuels with Commercial Diesel Lubricity Additives," presented at the WCX™ 17: SAE World Congress Experience, Mar. 2017, pp. 2017-01–0871. doi: 10.4271/2017-01-0871.
[18] N. Miyamoto, H. Ogawa, N. Md. Nurun, K. Obata, and T. Arima, "Smokeless, Low NOx, High Thermal Efficiency, and Low Noise Diesel Combustion with Oxygenated Agents as Main Fuel," presented at the International Congress & Exposition, Feb. 1998, p. 980506. doi: 10.4271/980506.
[19] K. F. Hansen et al., "Demonstration of a DME (Dimethyl Ether) Fuelled City Bus," presented at the CEC/SAE Spring Fuels & Lubricants Meeting & Exposition, Jun. 2000, pp. 2000-01–2005. doi: 10.4271/2000-01-2005.
[20] Y. Sato, S. Nozaki, and T. Noda, "The Performance of a Diesel Engine for Light Duty Truck Using a Jerk Type In-Line DME Injection System," presented at the 2004 SAE Fuels & Lubricants Meeting & Exhibition, Jun. 2004, pp. 2004-01–1862. doi: 10.4271/2004-01-1862.
[21] M. Oguma, S. Goto, and T. Watanabe, "Engine Performance and Emission Characteristics of DME Diesel Engine With Inline Injection Pump Developed for DME," presented at the 2004 SAE Fuels & Lubricants Meeting & Exhibition, Jun. 2004, pp. 2004-01–1863. doi: 10.4271/2004-01-1863.
[22] Hara T, Shimazaki N, Yanagisawa N, Seto T, Takase S, Tokumaru T, et al. Study of DME Diesel Engine for Low NOx and CO $_2$ Emission and Development of DME Trucks for Commercial Use. SAE Int J Fuels Lubr 2012;5(1):233–42.
[23] Lim YC, Jung JW, Suh HK. Effect of advanced intake valve closing on the thermochemical characteristics of the homogeneous combustion in a DME fueled HCCI engine. Fuel Aug. 2020;274:117700. https://doi.org/10.1016/j.fuel.2020.117700.
[24] Jang J, Lee Y, Cho C, Woo Y, Bae C. Improvement of DME HCCI engine combustion by direct injection and EGR. Fuel Nov. 2013;113:617–24. https://doi.org/10.1016/j.fuel.2013.06.001.
[25] Benajes J, Novella R, Pastor JM, Hernández-López A, Kokjohn S. Computational optimization of a combustion system for a stoichiometric DME fueled compression ignition engine. Fuel Jul. 2018;223:20–31. https://doi.org/10.1016/j.fuel.2018.03.022.
[26] Ji C, Liang C, Wang S. Investigation on combustion and emissions of DME/gasoline mixtures in a spark-ignition engine. Fuel Mar. 2011;90(3):1133–8. https://doi.org/10.1016/j.fuel.2010.11.033.
[27] Shi L, Ji C, Wang S, Cong X, Su T, Wang D. Combustion and emissions characteristics of a S.I. engine fueled with gasoline-DME blends under different spark timings. Fuel Jan. 2018;211:11–7. https://doi.org/10.1016/j.fuel.2017.09.019.
[28] Zhang HF, Seo K, Zhao H. Combustion and emission analysis of the direct DME injection enabled and controlled auto-ignition gasoline combustion engine operation. Fuel May 2013;107:800–14. https://doi.org/10.1016/j.fuel.2013.01.067.

[29] Cuoci A, Frassoldati A, Faravelli T, Ranzi E. OpenSMOKE++: An object-oriented framework for the numerical modeling of reactive systems with detailed kinetic mechanisms. Comput Phys Commun Jul. 2015;192:237–64. https://doi.org/10.1016/j.cpc.2015.02.014.
[30] Kaiser EW, Wallington TJ, Hurley MD, Platz J, Curran HJ, Pitz WJ, et al. Experimental and Modeling Study of Premixed Atmospheric-Pressure Dimethyl Ether−Air Flames. Chem A Eur J 2000;104(35):8194–206.
[31] Metcalfe WK, Burke SM, Ahmed SS, Curran HJ. A Hierarchical and Comparative Kinetic Modeling Study of C1–C2 Hydrocarbon and Oxygenated Fuels. Int J Chem Kinet 2013;45(10):638–75. https://doi.org/10.1002/kin.20802.
[32] K. D. Cung, A. A. Moiz, X. Zhu, and S.-Y. Lee, "Ignition Process and Flame Lift-Off Characteristics of dimethyl ether (DME) Reacting Spray," *Front. Mech. Eng.*, vol. 7, 2021, Accessed: Nov. 24, 2022. [Online]. Available: https://www.frontiersin.org/articles/10.3389/fmech.2021.547204.
[33] Jones WP, Launder BE. The prediction of laminarization with a two-equation model of turbulence. Int J Heat Mass Transf Feb. 1972;15(2):301–14. https://doi.org/10.1016/0017-9310(72)90076-2.
[34] Pope SB. An explanation of the turbulent round-jet/plane-jet anomaly. AIAA J Mar. 1978;16(3):279–81. https://doi.org/10.2514/3.7521.
[35] M. A. Patterson and R. D. Reitz, "Modeling the Effects of Fuel Spray Characteristics on Diesel Engine Combustion and Emission," presented at the International Congress & Exposition, Feb. 1998, p. 980131. doi: 10.4271/980131.
[36] Reitz RD. Modeling atomization processes in high-pressure vaporizing sprays. At Spray Technol Jan. 1987;3:309–37.
[37] H. Lehtiniemi, Y. Zhang, R. Rawat, and F. Mauss, "Efficient 3-D CFD Combustion Modeling with Transient Flamelet Models," presented at the SAE World Congress & Exhibition, Apr. 2008, pp. 2008-01–0957. doi: 10.4271/2008-01-0957.
[38] Burke U, Somers KP, O'Toole P, Zinner CM, Marquet N, Bourque G, et al. An ignition delay and kinetic modeling study of methane, dimethyl ether, and their mixtures at high pressures. Combust Flame 2015;162(2):315–30.
[39] Pelucchi M, Schmitt S, Gaiser N, Cuoci A, Frassoldati A, Zhang H, et al. On the influence of NO addition to dimethyl ether oxidation in a flow reactor. Combust Flame 2022:112464.
[40] Stagni A, Schmitt S, Pelucchi M, Frassoldati A, Kohse-Höinghaus K, Faravelli T. Dimethyl ether oxidation analyzed in a given flow reactor: Experimental and modeling uncertainties. Combust Flame Jun. 2022;240:111998. https://doi.org/10.1016/j.combustflame.2022.111998.
[41] Lee M, Fan Y, Ju Y, Suzuki Y. Ignition characteristics of premixed cool flames on a heated wall. Combust Flame Sep. 2021;231:111476. https://doi.org/10.1016/j.combustflame.2021.111476.
[42] A. Schirru *et al.*, "CFD Modeling of a DME CI Engine in Late-PCCI Operating Conditions," presented at the WCX SAE World Congress Experience, Detroit, Michigan, United States, Apr. 2023, pp. 2023-01–0203. doi: 10.4271/2023-01-0203.
[43] T. Lucchini, A. Della Torre, G. D'Errico, G. Montenegro, M. Fiocco, and A. Maghbouli, "Automatic Mesh Generation for CFD Simulations of Direct-Injection Engines," presented at the SAE 2015 World Congress & Exhibition, Apr. 2015, pp. 2015-01–0376. doi: 10.4271/2015-01-0376.
[44] Rakopoulos CD, Rakopoulos DC, Kosmadakis GM, Papagiannakis RG. Experimental comparative assessment of butanol or ethanol diesel-fuel extenders impact on combustion features, cyclic irregularity, and regulated emissions balance in heavy-duty diesel engine. Energy May 2019;174:1145–57. https://doi.org/10.1016/j.energy.2019.03.063.
[45] D'Errico G, Lucchini T, Contino F, Jangi M, Bai X-S. Comparison of well-mixed and multiple representative interactive flamelet approaches for diesel spray combustion modelling. Combust Theory Model Jan. 2014;18(1):65–88. https://doi.org/10.1080/13647830.2013.860238.
[46] Zhou Q, Lucchini T, D'Errico G, Novella R, García-Oliver JM, Lu X. CFD analysis of combustion and emission characteristics of primary reference fuels: from transient Diesel spray to heavy-duty engine. Fuel Oct. 2021;301:120994. https://doi.org/10.1016/j.fuel.2021.120994.
[47] Rakopoulos DC, Rakopoulos CD, Kosmadakis GM, Giakoumis EG. Exergy assessment of combustion and EGR and load effects in DI diesel engine using comprehensive two-zone modeling. Energy Jul. 2020;202:117685. https://doi.org/10.1016/j.energy.2020.117685.